scientific reports

OPEN

Application of artificial neural network and dynamic adsorption models to predict humic substances extraction from municipal solid waste leachate

Salimeh Rezaeinia[1], Ali Asghar Ebrahimi[1], Arash Dalvand[1], Mohammad Hassan Ehrampoush[1], Hossien Fallahzadeh[2] & Mehdi Mokhtari[1✉]

Sustainable municipal solid waste leachate (MSWL) management requires a paradigm shift from removing contaminants to effectively recovering resources and decreasing contaminants simultaneously. In this study, two types of humic substances, fulvic acid (FA) and humic acid (HA) were extracted from MSWL. HA was extracted using HCl and NaOH solution, followed by FA using a column bed under diversified operations such as flow rate, input concentration, and bed height. Also, this work aims to evaluate efficiency of Artificial Neural Network (ANN) and Dynamic adsorption models in predicting FA. With the flow rate of 0.3 mL/min, bed height of 15.5 cm, and input concentration of 4.27 g/mL, the maximum capacity of FA was obtained at 23.03 mg/g. FTIR analysis in HA and FA revealed several oxygen-containing functional groups including carboxylic, phenolic, aliphatic, and ketone. The high correlation coefficient value (R^2) and a lower mean squared error value (MSE) were obtained using the ANN, indicating the superior ability of ANN to predict adsorption capacity compared to traditional modeling.

Leachate produced in the municipal solid waste landfill (MSWL) is a by-product of decomposing biodegradable waste[1]. Each year, Municipal solid waste (MSW) landfills produce hundreds of thousands of cubic meters of leachates with a high organic content[2]. Currently, the movement toward a circular economy is focused on reusing materials formerly regarded as waste into valuable resources[3].

The successful recovery of value-added products from MSWL requires the utilization of efficient technologies[4]. Conventional MSWL treatment is frequently complicated, resulting in adverse environmental consequences and enforcing costs[5]. MSWL can be a potential resource for recovering highly value-added products[6,7]. Among the numerous substances that can be efficiently recovered from MSWL, humic substance (HS) is the most significant due to its multidirectional actions and extensive applications[8–10].

HS is a combination of polymeric, aromatic, and aliphatic acids produced by microbial decomposition of animal and plant waste. According to HS solubility in water at various pH values, they can be operationally divided into three parts: fulvic acid (FA), humic acid (HA), and humins (Hu)[11–13]. Due to their structure and abilities, HS improve soil conditioning, root development, nutrient uptake, and plant growth[14]. Recently, these substances have been recognized as treating organic pollutants (antibiotics, herbicides, fungicides, and other phenolic compounds) and heavy metals[15–17]. Therefore, finding ways to extract HS with high efficiency is necessary. Numerous extraction techniques for HS have been developed, including nonionic or ionic resin adsorption, membrane filtering, etc[18,19]. Resin adsorption techniques are one of the most popular approaches for FA extraction because of their simplicity, easy design, affordability, and low energy consumption.

FA can be extracted by resin adsorption, recommended by the International Humic Substances Society, into different chemical groups based on its hydrophobicity. The most commonly utilized resin is Suplite DAX-8 (previously known as XAD-8). Several studies have employed DAX-8 resin to extract FA from MSWL. Baccot

[1]Environmental Science and Technology Research Center, Department of Environmental Health Engineering, School of Public Health, Shahid Sadoughi University of Medical Sciences, Yazd, Iran. [2]Department of Biostatistics and Epidemiology, Research Center of Prevention and Epidemiology of Non-Communicable Disease, Shahid Sadoughi University of Medical Sciences, Yazd, Iran. ✉email: mokhtari@ssu.ac.ir; mhimokhtari@gmail.com

et al.[20] Extracted HS from MSWL as organic amendments to improve soil structure. Similar procedures were also employed to extract HA, FA, and other organic materials using DAX-8 columns[21].

Dynamic adsorption experiments can predict and model break-through curves (BTCs). They can also be easily scaled up for use in industry, making them a bridge between lab-scale experiments and real-world applications. In addition, since they can manage many solutions, they are more accurate for identifying design parameters in practical uses[22,23]. Several traditional mathematical models emerged for fixed-bed BTCs, including Thomas, Yoon-Nelson, and Bed Depth Service Time (BDST) models[24]. These models predict realistic adsorption efficiency without needing an experimental setup. Additionally, they give practical design information for columns[25]. However, there is a lack of information on the application of these models in the extraction of FA from MSWL using a fixed-bed.

In addition to the traditional models mentioned, the artificial neural network (ANN) model has been used to analyze the BTCs. ANN, a computer intelligence model influenced by biological and neurological processes, is increasingly popular for managing nonlinear processes[26]. ANN is widely recognized as a robust statistical tool due to a multitude of advantages. These advantages include the capacity to identify patterns through small modifications, the ability to approximate nonlinear systems without prior knowledge of variable relationships, simple use, and the capability to operate separately from conventional experimental designs[27]. The selection of ANN modeling was based on the features above to forecast and enhance the extraction of FS from MSWL. In recent years, its usage in the simulation adsorption processes has attracted wide attention[28]. However, little literature is reported on applying the ANN model in extracting FA with the fixed-bed column to our best knowledge.

The primary objective of this study was to establish extraction methods for obtaining HA and FA from MSWL. HA was initially isolated by applying the sample to HCl and NaOH chemicals. Subsequently, the FA was extracted utilizing a fixed-bed adsorption column under diversified operational variables such as flow rate, bed height, and input concentration. The experimental data were evaluated using the traditional Thomas, Yoon-Nelson, and BDST models and the ANN model. The models utilized to simulate and predict the extraction of FA using a fixed-bed column are novel aspects of this study. The results of this work could contribute to future efforts to extract HS from MSWL.

Material and methods

Landfill leachate sampling and characterization.
Characterization Landfill leachate and HS. The leachate samples were obtained from the MSW landfill site in Yazd city, Iran. The leachate samples were carried out in polyethylene containers directly from the landfill to the lab. The samples were stored at 4 °C immediately after arrival to decrease microbial activity. Characterizations of leachate samples are presented in Table 1.

Fourier transform infrared (FTIR) spectroscopy. A pellet was formed by mechanically pressing a mixture of one milligram of freeze-dried HA and FA with 100 mg of potassium bromide (KBr). The pellets were utilized for the purpose of analyzing the structure of HA and FA. FTIR spectra were obtained within the wavenumber range of $4000–400$ cm^{-1} with a resolution of 4 cm and 16 scans per acquisition[29].

Extraction protocol. The MSWL sample was filtered with 0.45 µm filter paper. After filtration, the sample was adjusted to pH below 2 with concentrated HCl and then refrigerated for 24 h to precipitate HA. After 24 h, solutions of 0.1 N NaOH were used to dissolve HA filtered through 0.45 µm filter paper. Following HA isolation, only FA and the hydrophilic fraction remained. The FA in the MSWL was extracted using a fixed-bed column, and the remaining stream was a nutrient-rich solution[30,31]. Following adsorption, the resins enriched with FA must be subsequently regenerated by 0.1 M NaOH, and the performance of resin reusability was assessed in this work[32].

Column experiments. A Pyrex glass tube column with a diameter of 10 mm and a height of 31 cm was used to study fixed-bed adsorption processes. The column was packed with DAX-8 resins, and the bottom was covered with glass wool to prevent the adsorbent from escaping (Fig. 1). The DAX 8 resin, obtained from Sigma-Aldrich, is classified as a hydrophilic acrylic ester. It exhibits a relatively low ion exchange capacity of 10^{-2} Mequiv/g, possesses an average pore size of 225 Å, and demonstrates a surface area of 160 m^2/g[33]. A peristaltic pump maintained a constant flow rate of HS solution of a specified concentration through the column. The bed heights were 6.3, 12.4, and 15.5 cm (equivalent to 2.07 g, 2.96 g, and 3.90 g of DAX-8 resins, respectively). Input HS concentrations were 4.27, 8.15, and 16.8 g/L. Also, the flow rates employed were 0.3, 1, and 2 mL/min. At periodic inter-

Parameter	Unit	Sample
pH	–	5.6
Conductivity	mS/cm	9.03
SUVA	L/mg m	2.98
DOC	mg/L	32,000
COD	mg/L	72,000
BOD	mg/L	19,000

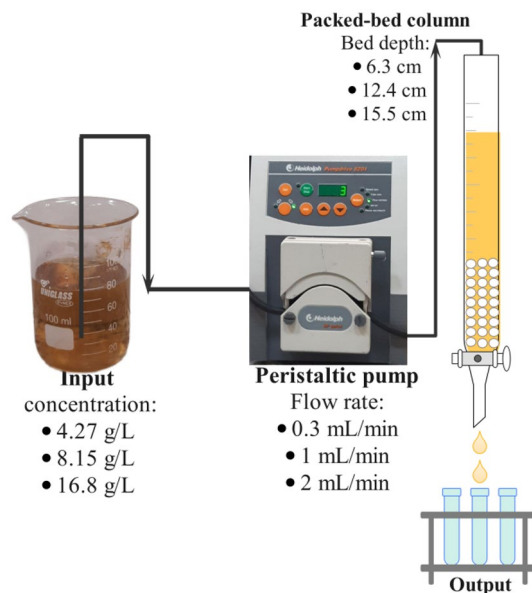**Table 1.** Characterization of MSWL used in this study.

Figure 1. Diagram of continues fixed bed column process.

vals, samples were collected to determine the remaining total organic carbon (TOC) concentration. The collection of samples continued until the concentrations of HS in the input and output leachate samples were equal.

Analyzing column data. The performance of fixed-bed adsorption columns was evaluated by analyzing the BTC$_s$. The BTC$_s$ were generally represented by the ratio C_t/C_0, where C_0 is the HS input concentration (mg/L), and C_t is the HS concentration at time t, respectively. The time at which output HS concentrations of MSWL samples reached 5% of the input HS concentration is defined as break-through time (t_b). Exhaustion time (t_e) occurs when output HS concentrations exceed 95% of input concentrations[34,35]. The experimental design parameters were determined for the BTC$_s$ of the column for FA adsorption onto DAX-8 resin. In this type of analysis, the top part of the BTC$_s$ represents the overall adsorbate weight (q_{total}, mg)[36], which can be calculated using Eq. (1):

$$q_{total} = \frac{QC_0}{1000} \int_0^{t_t} \left(1 - \frac{C_t}{C_0}\right) \tag{1}$$

where, Q represents the flow rate of HS (mL/min), C_0 is the HS input concentration (mg/L), C_t is the HS concentration at time t, and t is the time (min).

Using the following equation, the volume of output, V_{out} (mL), was computed as:

$$V_{out} = Q \times t_e \tag{2}$$

The equilibrium capacity to adsorption FA (q_e, mg/g) can be calculated using Eq. (3):

$$q_e = \frac{q_{total}}{M} \tag{3}$$

where, M (g) is the mass of the DAX-8 resin.

Finally, total FA extraction efficiency (%) can be determined as follows[37]:

$$R\% = \frac{1000 q_{total}}{C_0 Q t_e} \times 100\% \tag{4}$$

Break-through curve modeling. The fixed-bed column model might predict BTC$_s$ accurately in several different situations. These predictions allow us to identify operational conditions without conducting additional full-scale tests[26]. In this study, the BTC$_s$ were fitted using the Thomas, Yoon-Nelson, and BDST models.

Thomas model. The Thomas model is used to make predictions about the adsorption capacity. Also, it evaluates the BTC$_s$ performance by estimating the correlation between output concentration (C_t) and time (t)[38]. The nonlinear Thomas model is stated as follows[39]:

$$\frac{C_t}{C_0} = \frac{1}{1 + \exp\left(\frac{k_T q_T m}{Q} - k_T C_0 t\right)} \tag{5}$$

where, C_0 is the HS input concentration (mg/L), C_t is HS concentration at time t (mg/L), t is the time (min), K_T is the rate constant of Thomas (mL/mg min), Q denotes the flow rate (L/min), m is the mass of the DAX-8 resin (g), and q_T is the capacity of column adsorption (mg/g).

Yoon-Nelson model. The Yoon-Nelson model is frequently used in single adsorbate systems due to its ability to disregard adsorbate properties and adsorbent kinds[35]. The nonlinear Yoon-Nelson model can be described as:

$$\frac{C_t}{C_o} = \frac{1}{1 + \exp\left(k_{YN}\tau - k_{YN}t\right)} \tag{6}$$

where, K_{YN} is the rate constant of Yoon-Nelson (L/mg min), and τ is the time required for a 50% FA breakthrough (min).

BDST model. The most common and essential form of the model in the fixed-bed process is the BDST model, made by Hutchins and based on a proposal by Bohart and Adams[22]. It shows that the adsorption parameters at any bed height may be efficiently estimated using a linear correlation with the service time (t) and the bed depth (H)[40]. The BDST model can be expressed in a linear form as:

$$t = \frac{N_0}{C_0 \nu}H - \frac{1}{C_0 K_{BDST}}\ln\left(\frac{C_0}{C_t} - 1\right) \tag{7}$$

where, K_{BDST} is the rate constant of BDST (L/mg min), H is the bed depth (cm), N_0 is the capacity of the column adsorption (mg/L), and the velocity of the column when it is empty, denotes by ν (cm/min).

The error between the measured and predicted adsorption parameters can be obtained as:

$$\varepsilon = \frac{|x_{\exp} - x_{cal}|}{x_{\exp}} \times 100\% \tag{8}$$

where, $x_{\exp}$ indicates the empirical data and x_{cal} is calculated based on the adsorption model.

Error analysis. To determine the most suitable model based on its goodness of fit with the experimental data, it is imperative to conduct a thorough analysis of the data utilizing error analysis techniques. This study employed four distinct error analyses, namely the sum of the squares of the errors (SSE), the sum of absolute errors (SAE), average relative errors (ARE), and average relative standard error (ARS), to assess the magnitude of the error. The corresponding equations for each analysis can be found in Table S1.

Artificial neural network modeling. In this work, the ANN approach was utilized to assess the extraction performance of FA. The ANN model comprises different layers, including the input layer, hidden neurons, the output layer, the connection weight and biases, the activation function, and the summation nod[26,35]. The R2020a version of MATLAB software is used for implementing the ANN model. To this end, the experimental findings were divided into three categories: training (70%), validation (15%), and testing (15%). The Levenberg–Marquardt algorithm was applied to train the ANN. Also, the tan-sigmoid and linear transfer functions were used as the hidden and output layers activation functions, respectively.

The evaluation of the ANN model was conducted using performance metrics, including the Mean Absolute Error (MAE), Mean Squared Error (MSE), Root Mean Squared Error (RMSE), Coefficient of Determination (R^2), and Index of Agreement (IA). The equations for each of the performance measures are presented in Table S2.

Sensitivity analysis. The weight matrix approach was used to evaluate the relative importance of flow rate, input concentration, bed height, and total output time on the FA adsorption capacity. Garson developed this approach as[41]:

$$I_j = \frac{\sum_{m=1}^{m=N_h}\left(\left(\frac{\left|W_{jm}^{ih}\right|}{\sum_{k=1}^{Ni}\left|W_{km}^{ihh}\right|}\right) \times \left|W_{mn}^{ho}\right|\right)}{\sum_{k=1}^{k=Ni}\left\{\sum_{m=1}^{m=N_h}\left(\frac{\left|W_{km}^{ih}\right|}{\sum_{k=1}^{Ni}\left|W_{km}^{ih}\right|}\right) \times \left|W_{mn}^{ho}\right|\right\}} \times 100 \tag{9}$$

I_j is the relative importance of the jth input variable. Input variables are indicated by N_i, while N_h indicates hidden layer neurons. Connection weight is represented by W; input, hidden, and output layers are represented by the letters *i*, h, and o. Also, a number of input, hidden, and output neurons are represented by the letters k, m, and n.

Results and discussion

FTIR spectroscopy. The FTIR spectra for HA and FA extracted from MSWL are shown in Fig. 2. The spectra of the basic chemical structures of HA and FA revealed some identical and some different bands. The peak of 3378 cm^{-1} is found in the spectrum of HA, related to of phenolic and alcoholic O–H group of humic acid[42]. The HA and FA spectra contain a prominent peak at 2959–2863 cm^{-1} and are assigned to aliphatic C–H[43]. The high peak at 1560 cm^{-1} in the HA spectrum is attributed to C–O of carboxylic groups[44]. The band at about 1646 cm^{-1} in the FA spectrum may be ascribed to the presence of amide groups, quinones, and ketones[45]. The peak at 1416 and 1327 cm^{-1} in HA and FA is related to C–H, C–O stretching of polysaccharides[46]. The bands around 1104 and 1076 cm^{-1} were related to aromatic C–C (in ring) groups[47]. HA and FA exhibited peaks in the 929–607 cm^{-1} range are related to mineral components and aromatic C-H (out of plane) vibrations, respectively[48].

Influence of flow rate on FA extraction. The effect of flow rate on FA extraction was studied using input flow rates of 0.3, 1, and 2 mL/min at an input concentration of 4.27 g/L and a bed height of 15.5 cm. Figure 3a depicts the BTC$_s$ of FA at three flow rates, and Table 2 shows the analysis of break-through parameters for the continuous adsorption of FA. Increasing the flow rate decreased column break-through time (t_b). At flow rates of 0.3 mL/min and 2 mL/min, the t_b was 12.5 min and 2.77 min, respectively. In addition, a higher adsorption capacity was observed at lower flow rates (23.03, 20.47, and 19.27 mg/g for applied flow rates of 0.3, 1, and 2 mL/min, respectively). When the flow rate is low enough, the functional groups on the resin have adequate time to engage with the FA. The output concentration quickly reaches the initial value when the system flow rate increases, resulting in an early break-through[26,49].

Influence of bed height on FA extraction. The bed height of a continuous adsorption system is a critical design factor because it determines how long the solution stays in the column and how many adsorption sites are available[50]. Figure 3b shows the BTC$_s$ for FA adsorption for three different bed heights of 6.3, 12.4, and 15.5 cm with a flow rate of 0.3 mL/min and an input concentration of 4.27 g/L. As indicated in Table 2, the t_b increased from 4.16 to 12.5 min when the height of the bed rose from 6.3 to 15.5 cm. In addition, increasing the height of the column improved the adsorption capacity because more surface active places of DAX-8 resin were available for FA (21.66, 22.94, and 23.03 mg/g for applied bed high of 6.3, 12.4, and 15.5 cm, respectively). Increasing the bed height increases the time required to reach break-through and exhaustion[51]. Therefore, more extended break-through and exhaustion times were seen for the column with the deeper bed height because more DAX-8 adsorbent could be contained within the column, providing more functional groups for binding with FA[26]. The height of the adsorbent bed has a significant impact on the capture of FA during dynamic adsorption. It is evident that a larger bed column is preferable for FA isolation; however, the time needed should be carefully evaluated[35,49].

Influence of the input concentration on FA extraction. Three different values were employed to examine the Influence of input concentration on BTC$_s$ (4.27, 8.15, and 16.8 g/L), along with a bed height of 15.5 cm and flow rate of 0.3 mL/min. The results are shown in Table 2 and Fig. 3c. Increasing the input concentrations resulted in shorter break-through time and exhaustion times, which may have caused fast saturation of
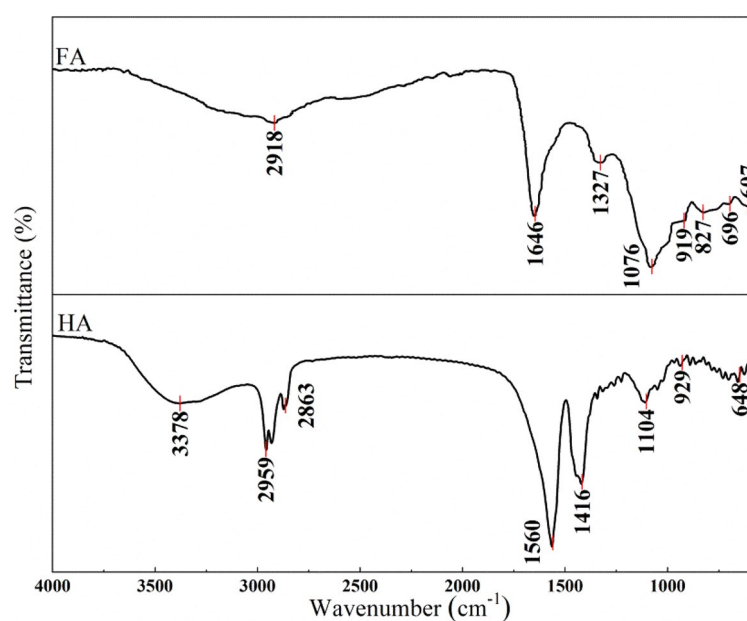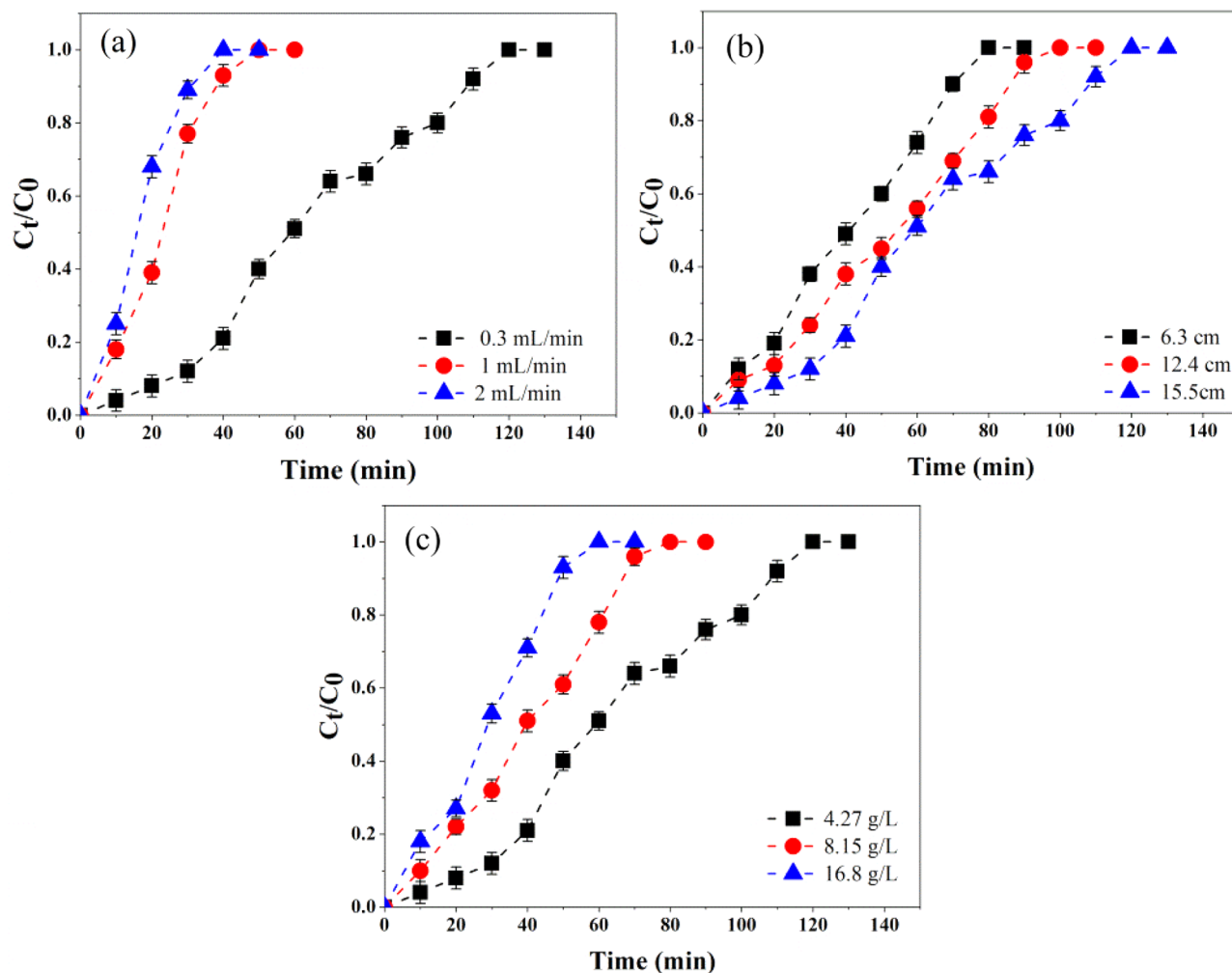

Figure 2. FTIR spectra of HA and FA from MSWL.

Figure 3. Effects of flow rate (**a**), bed height (**b**), and input concentration (**c**) on BTC$_s$ of FA adsorption.

Q (mL/min)	C$_0$ (mg/L)	H (cm)	t$_b$ (min)	t$_e$ (min)	V$_{eff}$ (mL)	q$_{total}$ (mg)	q$_e$ (mg/g)	R (%)
0.3	4270	15.5	12.5	113.75	34.13	81.47	23.03	61.63
1.0	4270	15.5	3.84	64.44	64.44	149.87	20.47	29.02
2.0	4270	15.5	2.77	54.99	109.98	233.99	19.27	16.07
0.3	4270	15.5	12.5	113.75	34.12	81.471	23.03	61.63
0.3	8150	15.5	5	77.85	23.35	102.69	23.82	48.82
0.3	16,800	15.5	2.77	62.85	18.85	157.75	24.55	30.23
0.3	4270	6.3	4.16	75.00	22.50	52.26	21.66	46.67
0.3	4270	12.4	5.5	89.33	26.80	66.48	22.94	59.33
0.3	4270	15.5	12.5	113.75	34.12	81.47	23.03	61.63

Table 2. The break-through parameters for FA adsorption at different operating conditions.

adsorption sites[52]. When the concentration increased from 4.27 to 16.8 g/L, the adsorption capacity increased from 23.03 to 24.55 mg/g (Table 2). Because the mass transfer driving power of the adsorption process increases with increasing input concentration, FA quickly saturates the adsorption sites on the resin[53]. The extraction rate was reduced from 61.63 to 30.23 with a higher input concentration. This is because as the input concentration increases, the output concentration increases. Simultaneously, a slower extraction rate results from a shorter break-through time.

Data modeling for BTC$_s$.   Adsorption kinetics and break-through parameters from the experimental data should be estimated using the Thomas, Yoon Nelson, and BDST models.

Thomas model.   The k_T and q_T for the Thomas model were obtained by fitting Eq. (5) to experimental data. Parameters and the results of fitting the Thomas model to the experimental data are displayed in Table 3 and Fig. 4, respectively. From Table 3, the R^2 levels (0.9857–0.9961) obtained from nonlinear fittings were relatively high, and the error levels (0.22–3.23) were low. By increasing the bed height, k_T valves decreased, whereas q_T values showed an increasing trend.

Conversely, by increasing the flow rate, the k_T values increased, but the value of q_T decreased. At high flow rates, FA only remains in the column for a short period, resulting in a decrease in adsorption capacity due to reduced transport rate from the surface of the adsorbent. A higher input HS concentration increased the q_0 level but decreased the k_T level. This is due to increased mass transfer driving power and duration of contact between the resin and FA[35]. The adsorption capacity obtained from experimental data ($q_{e,exp}$) is relatively close to the q_T.

Yoon-Nelson model.   The results of fitting the nonlinear Yoon-Nelson model to the experimental data of FA adsorption are shown in Fig. 5. The parameters K_{YN} and τ for the model are tabulated in Table 4. The values of R^2 are above 0.98, indicating that the Yoon-Nelson model correctly describes the FA adsorption process. The value of parameter K_{YN} showed an increasing trend with increasing flow rate and input concentration. However, τ levels decreased, indicating that the contact time is insufficient for FA and the required site for resin adsorption. K_{YN} levels gradually decrease with increasing adsorbent bed height, while τ levels showed an increasing trend. By increasing the mass of DAX-8, the contact of FA with the adsorbent bed is facilitated, resulting in a prolonged column adsorption process. It is seen that the τ_{cal} levels found with the Yoon-Nelson model and τ_{exp} levels in the column adsorption study are close to each other.

BDST model.   In order to calculate the K_{BDST} and N_0 in the BDST model, Eq. (7) used experimental data to plot the correlation between service time at the break-through point and packed-bed column depth[54]. Figure 6 shows the linear fit and model parameters of the BDST at 10%, 30%, 70%, and 90% break-through points, respectively (Table S3). The correlation coefficients of this model were obtained between. 9554 and 0.9652. By increasing the break-through point from 0.1 to 0.9, the N_0 value increased from 77.32 mg/L to 288.06 mg/L, and the K_{BDST} value reduced from 0.086 L/mg min to 0.024 L/mg min. It shows that the diffusion rate of FA from the leachate to the adsorbent has decreased due to the reduction of the concentration gradient[55].

Comparison of dynamic adsorption models.   In addition to the R^2, the optimal breakthrough models for FA adsorption in column studies were determined by employing different error functions, as indicated in Table S1. This study employed four distinct error analyses to evaluate the performance of three models: Thomas, Yoon-Nelson, and BDST model. The error values, namely SSE, SAE, ARE, and ARS, obtained for Thomas and Yoon Nelson's model are presented in Tables 3 and 4. Typically, smaller error values indicate a stronger alignment between the breakthrough model and the experimental data, suggesting a better fit. The error values decreased with the increase in initial concentrations, flow rate, and bed heights. The error value calculated using the Thomas and Yoon Nelson model is also minimal compared to the BDST model. In summary, the Yoon-Nelson and Thomas models effectively depicted the experimental findings.

ANN model.   In order to estimate the FA adsorption capacity, an ANN model with three feed-forward layers was developed, and the neural network was trained using the Levenberg–Marquardt optimization approach. Flow rate, input concentration, bed height, and total output time were used as the model inputs. On the other side, FA adsorption capacity was considered the output layer (Fig. 7a). Ranges of input and output variables and a graphical diagram of the optimized ANN are shown in Table S4 and Fig. S1, respectively. To determine the optimal number of neurons in the hidden layers, several simulations should be done with the different numbers of neurons, in which the lowest MSE is obtained[56]. The correlation between the MSE and the hidden layer neuron values is seen in Fig. 7b. The lowest MSE was obtained by nine neurons, selected as the optimized condition.

Q (mL/min)	C$_0$ (mg/L)	H (mL)	K$_T$/(mL/mg min)	q$_T$ (mg/g)	q$_{e, exp}$	R^2	SSE	SAE	ARE	ARS
0.3	4270	15.5	0.011	22.98	23.03	0.9858	0.295	0.543	0.136	0.039
1.0	4270	15.5	0.042	20.17	20.47	0.9961	0.018	0.136	0.047	0.019
2.0	4270	15.5	0.082	19.01	19.27	0.9954	0.015	0.121	0.019	0.009
0.3	4270	15.5	0.011	22.98	23.03	0.9858	0.295	0.543	0.136	0.039
0.3	8150	15.5	0.010	23.51	23.82	0.9880	0.117	0.341	0.056	0.019
0.3	16,800	15.5	0.009	24.15	24.55	0.9901	0.066	0.256	0.066	0.025
0.3	4270	6.3	0.019	20.96	21.66	0.9857	0.125	0.353	0.055	0.018
0.3	4270	12.4	0.012	22.61	22.94	0.9870	0.176	0.419	0.062	0.019
0.3	4270	15.5	0.011	22.98	23.03	0.9858	0.295	0.543	0.136	0.039

Table 3. Fitting the results of the dynamic adsorption model by Thomas.
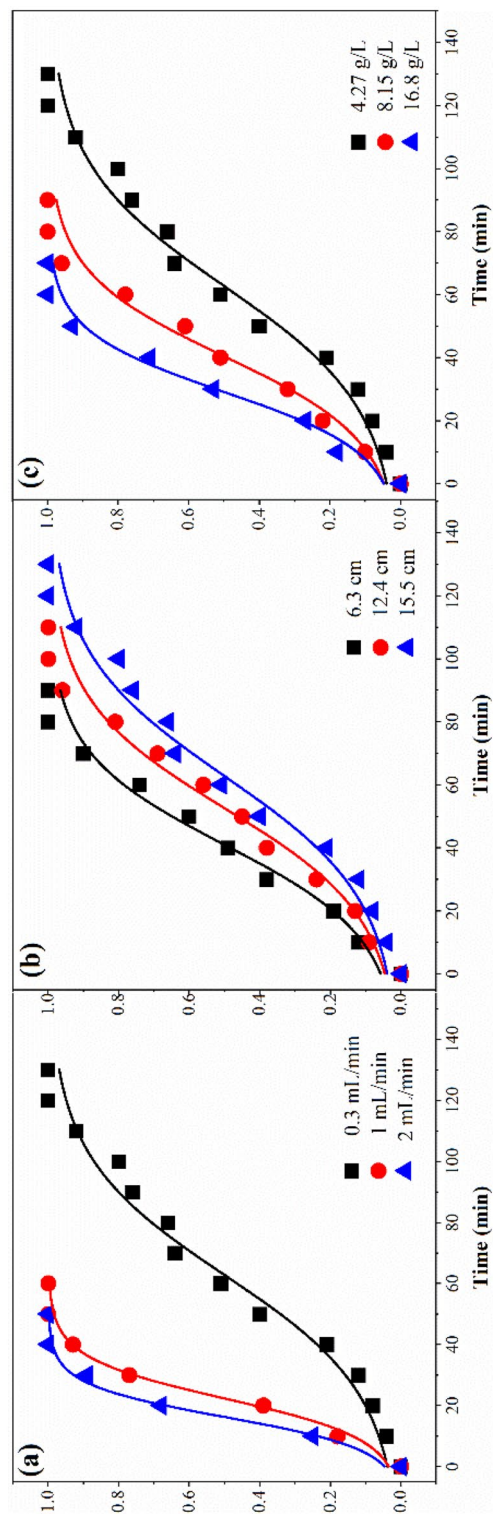
Figure 4. The predicted BTC$_s$ for FA adsorption by the Thomas model, (**a**) flow rate; (**b**) bed height; (**c**) input concentration.
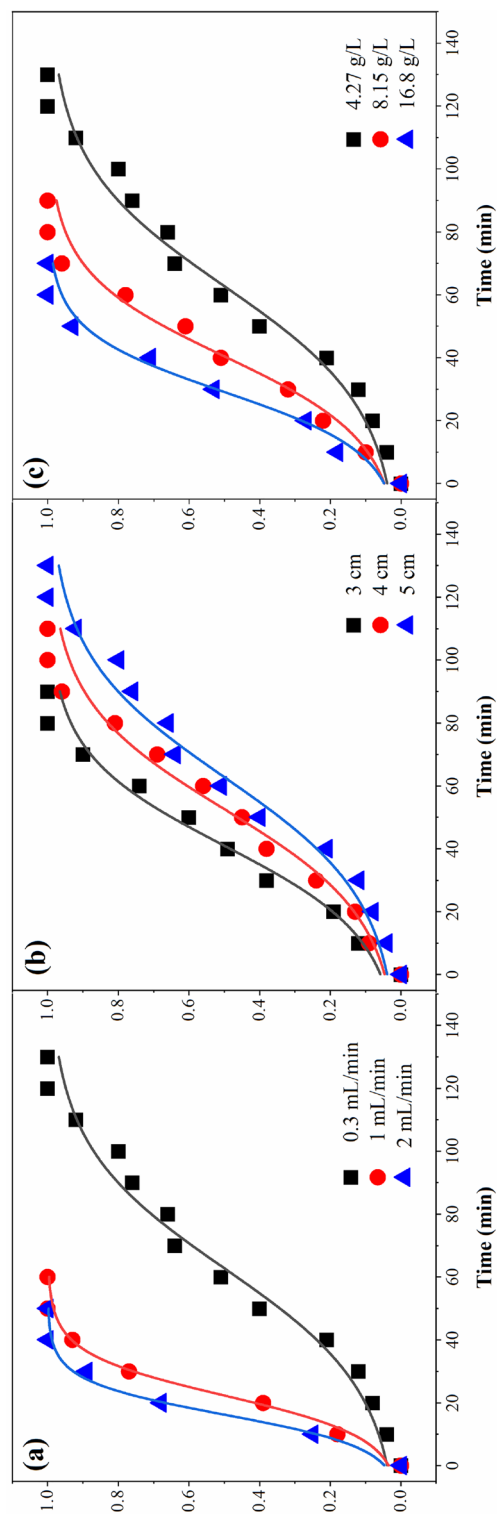
8

Figure 5. The predicted BTCs for FA adsorption by the Yoon-Nelson model, (**a**) flow rate; (**b**) bed height; (**c**) input concentration.

Q (mL/min)	C$_0$ (mg/L)	H (mL)	K$_{YN}$/10^{-3} (mL/mg min)	τ_{cal} (min)	τ_{exp} (min)	R^2	SSE	SAE	ARE	ARS
0.3	4270	15.5	0.051	64.02	64.47	0.9858	0.295	0.543	0.136	0.039
1.0	4270	15.5	0.092	37.77	37.09	0.9961	0.018	0.136	0.047	0.019
2.0	4270	15.5	0.095	38.95	39.21	0.9954	0.015	0.121	0.019	0.009
0.3	4270	15.5	0.051	64.02	64.47	0.9858	0.295	0.543	0.136	0.039
0.3	8150	15.5	0.062	48.39	48.74	0.9880	0.117	0.341	0.056	0.019
0.3	16,800	15.5	0.063	47.46	46.67	0.9901	0.066	0.256	0.066	0.025
0.3	4270	6.3	0.067	41.49	41.41	0.9857	0.125	0.353	0.055	0.018
0.3	4270	12.4	0.059	51.35	51.92	0.9870	0.176	0.419	0.062	0.019
0.3	4270	15.5	0.051	64.02	67.47	0.9858	0.295	0.543	0.136	0.039

Table 4. Fitting the results of the dynamic adsorption model by Yoon-Nelson.
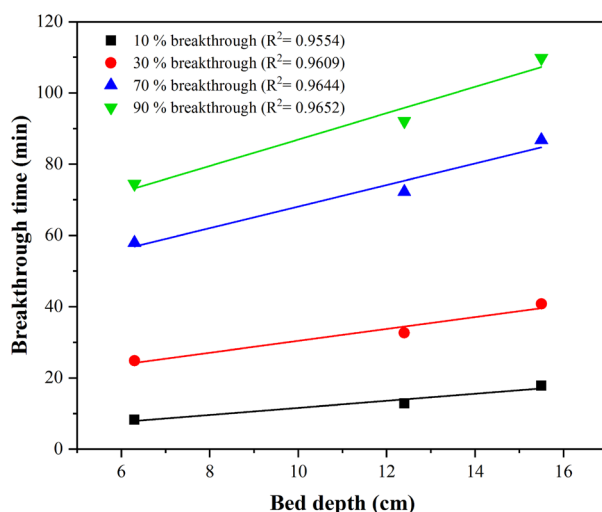
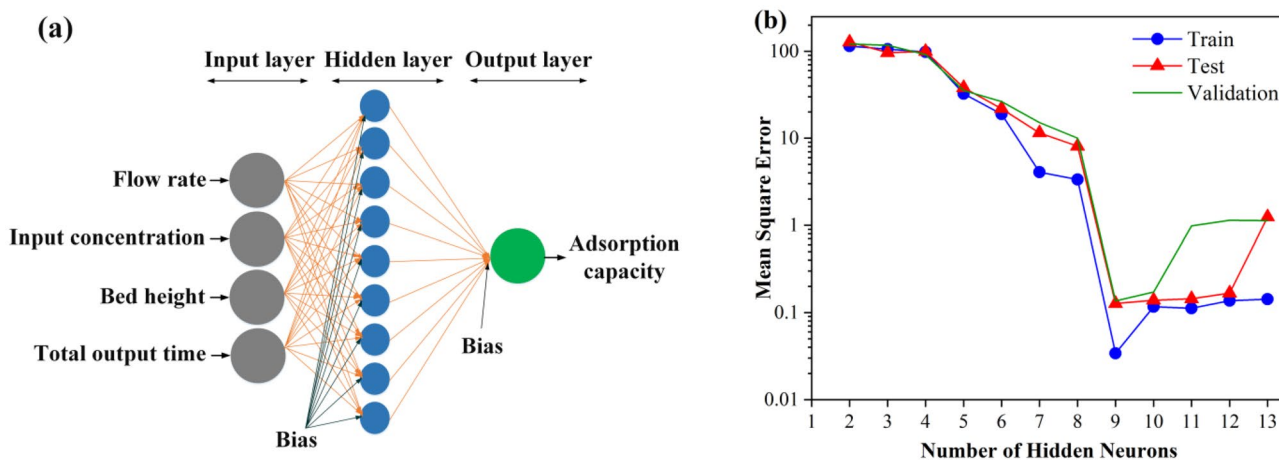**Figure 6.** BDST model result of FA adsorption process at different break-through points.

Figure 7. (**a**) Schematic diagram of ANN in this study; (**b**) Effect of hidden neurons.

The relationship between the experimental data and the predicted data by the ANN model is shown in Fig. 8a. Also, Experimental and predicted data are shown in Table S5. R^2, MSE, RMSE, MAE, and IA parameters for this model are 0.999, 0.624, 0.790, 0.625 and 0.488, respectively. Therefore, it seems that the ANN model can accurately predict the extraction of FA in the fixed-bed column.
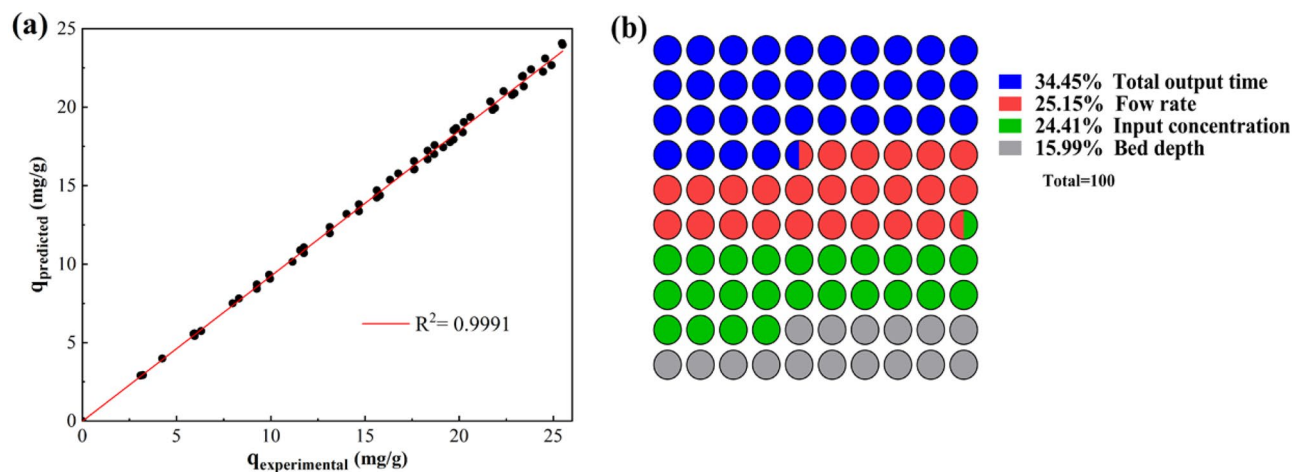
Figure 8. (**a**) Correlation between adsorption capacity of FA obtained from ANN model and experiments; (**b**) the relative importance of each input parameter.

Sensitivity analysis. Sensitivity analysis was utilized to estimate the level of influence of operating parameters on the Extraction of FA. Connecting the weight value of the model enlisted in Table S6 data. The importance of input parameters is evaluated by Eq. (9). The relative importance of each input variable is shown in Fig. 8b. The total output time, with a relative importance of 34.45%, was found to be the most influential variable in the adsorption of FA. After that, the relative importance of flow rate, input concentration, and column height was obtained at 25.15%, 24.41%, and 15.99%, respectively. In the process of FA adsorption from MSWL, achieving the larger adsorption capacity requires more time, so it is considered the most influential variable.

Sorbent regeneration. In order to extract the FA on a large-scale practically, the column must be able to be used more than once. Only in this way, the costs of the extraction process can be kept low[57]. This study evaluated the effectiveness of saturated DAX-8 resin by three adsorption–desorption cycles using 0.1 M NaOH solution. Figure 9 shows the BTC$_s$ for these three regeneration cycles. The break-through time, exhaustion time, adsorption capacity, and extraction rate of each cycle are tabulated in Table S7. As can be seen, the break-through and exhaustion time in cycles 1–3 gradually decreased from 10.44 to 7.58 min and 97.21 to 83.42 min, respectively. Also, due to decreasing the break-through and exhaustion time after three adsorption–desorption cycles, the adsorption capacity and the extraction rate decreased from 17.21 to 13.11 mg/g and 49.21 to 31.47%, respectively. It should be noted that the regeneration efficiency was above 50% after three cycles. This shows that DAX-8 resin has the potential to be reused.
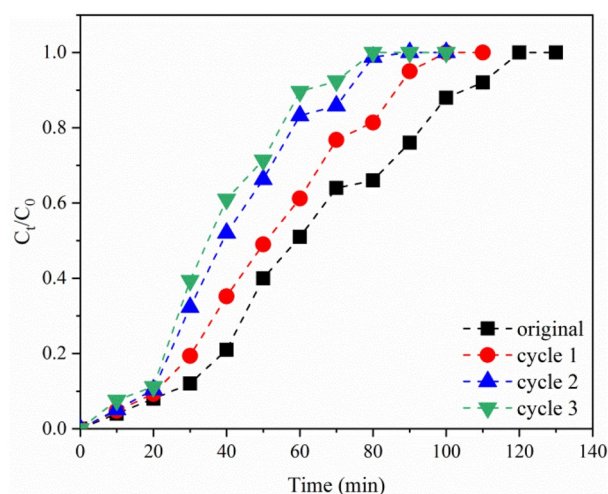

Figure 9. The experimental BTC$_s$ for FA adsorption during regeneration cycles.

Conclusions

Based on this research's objective, HA and FA extraction from MSWL was performed effectively. The extracted material was characterized by FTIR analyses, which confirmed functional groups, including carboxylic, phenolic, aliphatic, and ketone.

The influence of diversified operational variables (flow rate, input concentration, and bed height) were investigated on column performance. The break-through time, exhaustion times, adsorption capacity, and extraction rate increased with a high bed height and a low flow rate.

By increasing the input concentration, the adsorption capacity of FA increases while the break-through time, exhaustion times, and extraction rate decrease. The models proposed by Thomas and Yoon-Nelson exhibited a strong fit to the experimental column data, suggesting their ability to accurately estimate the breakthrough curves (BTCs). The BDST model demonstrated a strong linear correlation between bed depth and break-through point, indicating its potential suitability for column design. Based on the statistical analysis conducted, it was determined that the experimental data exhibited a strong fit with the proposed model. The ANN model had the best correlation coefficients and the smallest MSE compared to the other studied models. With relative importance of 34.45%, the total output time ranked as the most important of all the parameters. The relative importance of the flow rate, input concentration, and column height was 25.15%, 24.41%, and 15.99%, respectively. Exhausted column beds were regenerated, and adsorption capacities were changed from 41.29 to 31.47 mg/g after three cycles, indicating a relatively practical value to extract FA from MSWL.

Data availability

The datasets used and/or analyzed during the current study are available from the corresponding author on reasonable request.

References

1. Nanda, S. & Berruti, F. Municipal solid waste management and landfilling technologies: A review. *Environ. Chem. Lett.* **19**, 1433–1456 (2021).
2. Sharma, P. & Kumar, S. Characterization and phytotoxicity assessment of organic pollutants in old and fresh municipal solid wastes at open dump site: A case study. *Environ. Technol. Innov.* **24**, 101938 (2021).
3. Puntillo, P., Gulluscio, C., Huisingh, D. & Veltri, S. Reevaluating waste as a resource under a circular economy approach from a system perspective: Findings from a case study. *Bus. Strateg. Environ.* **30**, 968–984 (2021).
4. Cheng, S. Y. *et al.* Landfill leachate wastewater treatment to facilitate resource recovery by a coagulation-flocculation process via hydrogen bond. *Chemosphere* **262**, 127829 (2021).
5. Iskander, S. M., Brazil, B., Novak, J. T. & He, Z. Resource recovery from landfill leachate using bioelectrochemical systems: Opportunities, challenges, and perspectives. *Biores. Technol.* **201**, 347–354 (2016).
6. Kurniawan, T. A. *et al.* Resource recovery from landfill leachate: An experimental investigation and perspectives. *Chemosphere* **274**, 129986 (2021).
7. Kurniawan, T. A. *et al.* Resource recovery toward sustainability through nutrient removal from landfill leachate. *J. Environ. Manage.* **287**, 112265 (2021).
8. Ye, W. *et al.* Sustainable management of landfill leachate concentrate through recovering humic substance as liquid fertilizer by loose nanofiltration. *Water Res.* **157**, 555–563 (2019).
9. Gu, N., Liu, J., Ye, J., Chang, N. & Li, Y.-Y. Bioenergy, ammonia and humic substances recovery from municipal solid waste leachate: A review and process integration. *Biores. Technol.* **293**, 122159 (2019).
10. Lin, J. *et al.* Sustainable management of landfill leachate concentrate via nanofiltration enhanced by one-step rapid assembly of metal-organic coordination complexes. *Water Res.* **204**, 117633 (2021).
11. Guo, X.-X., Liu, H.-T. & Wu, S.-B. Humic substances developed during organic waste composting: Formation mechanisms, structural properties, and agronomic functions. *Sci. Total Environ.* **662**, 501–510 (2019).
12. Łomińska-Płatek, D. & Anielak, A. M. Quantitative balance and analysis of fulvic acids changes in the process of municipal sewage treatment. *Water Resour. Ind.* **26**, 100155 (2021).
13. Nguyen, H.V.-M., Lee, H.-S., Lee, S.-Y., Hur, J. & Shin, H.-S. Changes in structural characteristics of humic and fulvic acids under chlorination and their association with trihalomethanes and haloacetic acids formation. *Sci. Total Environ.* **790**, 148142 (2021).
14. Meng, F., Huang, Q., Yuan, G., Cai, Y. & Han, F. X. *New Trends in Removal of Heavy Metals from Industrial Wastewater* 131–160 (Elsevier, 2021).
15. Xu, P. *et al.* The broad application and mechanism of humic acids for treating environmental pollutants: Insights from bibliometric analysis. *J. Clean. Prod.* **337**, 130510 (2022).
16. Lipczynska-Kochany, E. Humic substances, their microbial interactions and effects on biological transformations of organic pollutants in water and soil: A review. *Chemosphere* **202**, 420–437 (2018).
17. Piccolo, A., Spaccini, R., De Martino, A., Scognamiglio, F. & di Meo, V. Soil washing with solutions of humic substances from manure compost removes heavy metal contaminants as a function of humic molecular composition. *Chemosphere* **225**, 150–156 (2019).
18. Kleber, M. & Lehmann, J. Humic substances extracted by alkali are invalid proxies for the dynamics and functions of organic matter in terrestrial and aquatic ecosystems. *J. Environ. Qual.* **48**, 207–216 (2019).
19. Mahler, C. F., Dal Santo Svierzoski, N. & Bernardino, C. A. R. Chemical characteristics of humic substances in nature. in *Humic Substance* (2021).
20. Baccot, C., Pallier, V., Thom, M. T., Thuret-Benoist, H. & Feuillade-Cathalifaud, G. Valorization of extracted organic matter from municipal solid waste leachate: Application to soils from France and Togo. *Waste Manage.* **102**, 161–169 (2020).
21. Vithanage, M., Wijesekara, H. & Mayakaduwa, S. Isolation, purification and analysis of dissolved organic carbon from Gohagoda uncontrolled open dumpsite leachate, Sri Lanka. *Environ. Technol.* **38**, 1610–1618 (2017).
22. Chen, C. *et al.* Dynamic adsorption models and artificial neural network prediction of mercury adsorption by a dendrimer-grafted polyacrylonitrile fiber in fixed-bed column. *J. Clean. Prod.* **310**, 127511 (2021).
23. Naddafi, K., Rastkari, N., Nabizadeh, R., Saeedi, R. & Gholami, M. Removal of 2, 4, 6-trichlorophenol from aqueous solutions by cetylpyridinium bromide (CPB)-modified zeolite in batch and continuous systems. *Desalin. Water Treat.* **86**, 131–138 (2017).

24. Chu, K. H. Breakthrough curve analysis by simplistic models of fixed bed adsorption: In defense of the century-old Bohart-Adams model. *Chem. Eng. J.* **380**, 122513 (2020).
25. Hethnawi, A., Manasrah, A. D., Vitale, G. & Nassar, N. N. Fixed-bed column studies of total organic carbon removal from industrial wastewater by use of diatomite decorated with polyethylenimine-functionalized pyroxene nanoparticles. *J. Colloid Interface Sci.* **513**, 28–42 (2018).
26. Chen, S., Bai, S., Ya, R., Du, C. & Ding, W. Continuous silicic acid removal in a fixed-bed column using a modified resin: Experiment investigation and artificial neural network modeling. *J. Water Process Eng.* **49**, 102937 (2022).
27. Juela, D., Vera, M., Cruzat, C., Astudillo, A. & Vanegas, E. A new approach for scaling up fixed-bed adsorption columns for aqueous systems: A case of antibiotic removal on natural adsorbent. *Process Saf. Environ. Prot.* **159**, 953–963 (2022).
28. Chowdhury, S. & Saha, P. D. Artificial neural network (ANN) modeling of adsorption of methylene blue by NaOH-modified rice husk in a fixed-bed column system. *Environ. Sci. Pollut. Res.* **20**, 1050–1058 (2013).
29. Raguraj, S., Kasim, S., Jaafar, N. M., Nazli, M. H. & Amali, R. K. A. A comparative study of tea waste derived humic-like substances with lignite-derived humic substances on chemical composition, spectroscopic properties and biological activity. *Environ. Sci. Pollut. Res.* **29**, 60631–60640 (2022).
30. Mallick, S. P. *Method Development for Aquatic Humic Substance Isolation and Its Application to Landfill Leachate* (Lamar University-Beaumont, 2017).
31. Chen, C.-Y., Li, W.-T. & Pan, S.-Y. Performance evaluation of cascade separation for a humic substance and nutrient recovery from piggery wastewater toward a circular bioeconomy. *ACS Sustain. Chem. Eng.* **9**, 8115–8124 (2021).
32. Liu, H., Li, Y., Yang, H., Siddique, M. S. & Yu, W. The characters of dissolved organic matters from litter-mimic with the different humification states and their effects on drinking water treatment processes. *Sci. Total Environ.* **861**, 160470 (2023).
33. Hughes, D., Holliman, P., Jones, T., Butler, A. J. & Freeman, C. Rapid, semi-automated fractionation of freshwater dissolved organic carbon using DAX 8 (XAD 8) and XAD 4 resins in Tandem. *Nat. Sci.* **8**, 487–498 (2016).
34. Aslam, M. M. A., Den, W. & Kuo, H.-W. Removal of hexavalent chromium by encapsulated chitosan-modified magnetic carbon nanotubes: Fixed-bed column study and modelling. *J. Water Process Eng.* **42**, 102143 (2021).
35. Bai, S., Li, J., Ding, W., Chen, S. & Ya, R. Removal of boron by a modified resin in fixed bed column: Breakthrough curve analysis using dynamic adsorption models and artificial neural network model. *Chemosphere* **296**, 134021 (2022).
36. Hu, A. *et al.* Phosphate recovery with granular acid-activated neutralized red mud: Fixed-bed column performance and breakthrough curve modelling. *J. Environ. Sci.* **90**, 78–86 (2020).
37. Feizi, F., Sarmah, A. K. & Rangsivek, R. Adsorption of pharmaceuticals in a fixed-bed column using tyre-based activated carbon: Experimental investigations and numerical modelling. *J. Hazard. Mater.* **417**, 126010 (2021).
38. Dalhat, M., Mu'azu, N. D. & Essa, M. H. Generalized decay and artificial neural network models for fixed-Bed phenolic compounds adsorption onto activated date palm biochar. *J. Environ. Chem. Eng.* **9**, 104711 (2021).
39. Han, R., Wang, Y., Zou, W., Wang, Y. & Shi, J. Comparison of linear and nonlinear analysis in estimating the Thomas model parameters for methylene blue adsorption onto natural zeolite in fixed-bed column. *J. Hazard. Mater.* **145**, 331–335 (2007).
40. Callery, O. & Healy, M. G. Predicting the propagation of concentration and saturation fronts in fixed-bed filters. *Water Res.* **123**, 556–568 (2017).
41. Hosseinzadeh, A. *et al.* Application of artificial neural network and multiple linear regression in modeling nutrient recovery in vermicompost under different conditions. *Biores. Technol.* **303**, 122926 (2020).
42. Nuzzo, A., Buurman, P., Cozzolino, V., Spaccini, R. & Piccolo, A. Infrared spectra of soil organic matter under a primary vegetation sequence. *Chem. Biol. Technol. Agric.* **7**, 1–12 (2020).
43. Guzeva, A. Geochemical features of humic acids extracted from sediments of urban lakes of the Arctic. *Environ. Monit. Assess.* **194**, 749 (2022).
44. Chen, H., Li, Q., Wang, M., Ji, D. & Tan, W. XPS and two-dimensional FTIR correlation analysis on the binding characteristics of humic acid onto kaolinite surface. *Sci. Total Environ.* **724**, 138154 (2020).
45. Verrillo, M. *et al.* Antiflammatory activity and potential dermatological applications of characterized humic acids from a lignite and a green compost. *Sci. Rep.* **12**, 2152 (2022).
46. Savy, D., Cozzolino, V., Vinci, G., Nebbioso, A. & Piccolo, A. Water-soluble lignins from different bioenergy crops stimulate the early development of maize (*Zea mays*, L.). *Molecules* **20**, 19958–19970 (2015).
47. Santos, J. *et al.* High-value compounds obtained from grape canes (*Vitis vinifera* L.) by steam pressure alkali extraction. *Food Bioprod. Process.* **133**, 153–167 (2022).
48. Monda, H., Cozzolino, V., Vinci, G., Spaccini, R. & Piccolo, A. Molecular characteristics of water-extractable organic matter from different composted biomasses and their effects on seed germination and early growth of maize. *Sci. Total Environ.* **590**, 40–49 (2017).
49. Talat, M. *et al.* Effective removal of fluoride from water by coconut husk activated carbon in fixed bed column: Experimental and breakthrough curves analysis. *Groundw. Sustain. Dev.* **7**, 48–55 (2018).
50. Alardhi, S. M., Albayati, T. M. & Alrubaye, J. M. Adsorption of the methyl green dye pollutant from aqueous solution using mesoporous materials MCM-41 in a fixed-bed column. *Heliyon* **6**, e03253 (2020).
51. Ansari, A., Nadres, E. T., Đỗ, M. & Rodrigues, D. F. Investigation of the removal and recovery of nitrate by an amine-enriched composite under different fixed-bed column conditions. *Process Saf. Environ. Prot.* **150**, 365–372 (2021).
52. Abdolali, A. *et al.* Application of a breakthrough biosorbent for removing heavy metals from synthetic and real wastewaters in a lab-scale continuous fixed-bed column. *Biores. Technol.* **229**, 78–87 (2017).
53. Girish, C. & Murty, V. R. Adsorption of phenol from aqueous solution using Lantana camara, forest waste: Packed bed studies and prediction of breakthrough curves. *Environ. Process.* **2**, 773–796 (2015).
54. Du, Z., Zheng, T. & Wang, P. Experimental and modelling studies on fixed bed adsorption for Cu(II) removal from aqueous solution by carboxyl modified jute fiber. *Powder Technol.* **338**, 952–959 (2018).
55. Fallah, N. & Taghizadeh, M. Continuous fixed-bed adsorption of Mo(VI) from aqueous solutions by Mo(VI)-IIP: Breakthrough curves analysis and mathematical modeling. *J. Environ. Chem. Eng.* **8**, 104079 (2020).
56. Gupta, K. N. & Kumar, R. Fixed bed utilization for the isolation of xylene vapor: Kinetics and optimization using response surface methodology and artificial neural network. *Environ. Eng. Res.* **26**, 200105 (2021).
57. Şentürk, İ & Alzein, M. Adsorptive removal of basic blue 41 using pistachio shell adsorbent-performance in batch and column system. *Sustain. Chem. Pharm.* **16**, 100254 (2020).

Acknowledgements

Author contributions
S.R. performed the experiments and drafted the manuscript. A.A.E. and A.D. analyzed the experimental results. M.H.E. and H.F. interpreted the data. M.M. contributed to design experiments and material preparation and read and approved the final manuscript. All authors commented on previous versions of the manuscript.

Competing interests
The authors declare no competing interests.

Additional information
Supplementary Information The online version contains supplementary material available at https://doi.org/10.1038/s41598-023-39373-2.

Correspondence and requests for materials should be addressed to M.M.

Reprints and permissions information is available at www.nature.com/reprints.

Publisher's note Springer Nature remains neutral with regard to jurisdictional claims in published maps and institutional affiliations.